Fluids and Barriers of the CNS

RESEARCH

Open Access

Rutin ameliorates stress–induced blood–brain barrier dysfunction and cognitive decline via the endothelial HDAC1–Claudin–5 axis

Zhao–Wei Sun[1†], Zhao–Xin Sun[1,2†], Yun Zhao[1†], Ling Zhang[1], Fang Xie[1], Xue Wang[1], Jin–Shan Li[1,2], Mao–Yang Zhou[1], Hong Feng[2*] and Ling–Jia Qian[1*]

Abstract

Background Emerging evidence suggests that chronic stress compromises blood—brain barrier (BBB) integrity by disrupting brain microvascular endothelial cells (BMECs), contributing to the development of cognitive impairments. Thus, targeting the BBB is expected to be a promising treatment strategy. The biological function of rutin has been investigated in neurological disorders; however, its regulatory role in stress–induced BBB damage and cognitive decline and the underlying mechanisms remain elusive.

Methods In a chronic unpredictable mild stress (CUMS) mouse model, a fluorescent dye assay and behavioral tests, including a novel object recognition test and Morris water maze, were performed to evaluate the protective effects of rutin on BBB integrity and cognition. The effects of rutin on BMEC function were also investigated in hCMEC/D3 cells (a human brain microvascular endothelial cell line) in vitro. Furthermore, the molecular mechanisms by which rutin restores BBB endothelium dysfunction were explored via RNA–seq, quantitative real–time PCR, western blotting, immunofluorescence and chromatin immunoprecipitation. Finally, biotinylated tumor necrosis factor–α (TNF–α) was employed to test the influence of rutin on the ability of circulating TNF–α to cross the BBB.

Results We identified that rutin attenuated BBB hyperpermeability and cognitive impairment caused by the 8–week CUMS procedure. Moreover, rutin promoted the proliferation, migration and angiogenesis ability of BMECs, and the integrity of the cellular monolayer through positively regulating the expression of genes involved. Furthermore, rutin impeded histone deacetylase 1 (HDAC1) recruitment and stabilized H3K27ac to increase Claudin–5 protein levels. Ultimately, normalization of the hippocampal HDAC1—Claudin–5 axis by rutin blocked the infiltration of circulating TNF–α into the brain parenchyma and alleviated neuroinflammation.

Conclusions This work establishes a protective role of rutin in regulating BMEC function and BBB integrity, and reveals that rutin is a potential drug candidate for curing chronic stress–induced cognitive deficits.

Keywords Rutin, Stress–induced cognitive decline, BBB, BMEC function, Claudin–5, H3K27ac modification

†Zhao–Wei Sun, Zhao–Xin Sun and Yun Zhao have contributed equally to this work.

*Correspondence:
Hong Feng
hong_feng2009@126.com
Ling–Jia Qian
stressqian@163.com

Introduction

Stress is a nonspecific and adaptive response caused by social and environmental factors and is correlated with various neurodegenerative diseases. Specifically, substantial evidence has recognized chronic stress as a risk factor for the development of cognitive impairments and even dementia [1, 2]. In humans, proneness to distress increases the risk of developing dementia by 2.4 times [3]; Alzheimer's disease (AD) patients present elevated levels of plasma cortisol, which is a typical endocrine marker of chronic stress [4]. Thus, there is an urgent need to elucidate the mechanism underlying stress–induced cognitive decline to explore potential therapeutic strategies.

Microvascular disruption is a remarkable feature of stress–induced cognitive impairments, and specifically, defective blood–brain barrier (BBB) function appears to be a key driver of pathology [5–7]. The BBB, which is composed of brain microvascular endothelial cells (BMECs) lining brain capillaries, maintains an environment that allows neurons to function properly [8]. Numerous studies in animal models of cognitive decline have revealed a series of BBB abnormalities, including BMEC dysfunction, tight junction (TJ) loss and aberrant molecule transport [9, 10]. Given that the BBB is a key modulator of brain homeostasis, great efforts have been made to discover effective drugs that can directly stabilize BMEC integrity and BBB function. To date, however, no such compound exists in clinic.

Many natural products have progressed toward the prevention and treatment of stress–induced BBB breakdown and cognitive decline [11–13]. Rutin (quercetin–3–O–rutinoside), a flavonoid glycoside commonly found in numerous plants, possesses various pharmacological properties, including anti–inflammatory, antioxidative, immunomodulatory and antidepressant activities [14, 15]. Recent studies suggest that rutin and its derivatives can defend against neuroinflammation, stimulate neurogenesis and ameliorate spatial memory in several models of neurodegenerative diseases [11, 16, 17]. Meanwhile, evidence has indicated that rutin can inhibit the oxidative stress and apoptosis of endothelial cells [18, 19]. Also, rutin is able to improve cerebrovascular damage caused by ischemia–reperfusion [20, 21], suggesting that it plays a potential role in protecting neurovascular function. However, the effects of rutin on chronic stress–induced BBB damage and cognitive decline and the underlying mechanisms are not fully understood.

In the present study, we observed that rutin enhanced the proliferation, migration and angiogenesis capacity of BMECs to promote its integrity. Moreover, rutin facilitated the expression of the TJ protein Claudin–5 by eliminating the inhibitory effect of histone deacetylase 1 (HDAC1). Finally, the ability of rutin to restore BBB integrity restricted the aggregation of peripheral TNF–α in the hippocampus to alleviate neuroinflammation and cognitive dysfunction, indicating that rutin is a promising drug candidate for the clinical treatment of stress–induced cognitive impairments.

Materials and methods

Mice

Six–week–old male C57BL/6 mice (20–22 g) were obtained from the Laboratory Animal Center of the Academy of Military Sciences (AMS) and were provided ad libitum access to food and water. The standard 12–h light/12–h dark cycle was changed only during the course of the stress intervention. All mouse experiments complied with the National Institutes of Health Guide for the Care and Use of Laboratory Animals (NIH Publication No. 8023) and were approved by the Animal Care and Use Committee at the AMS (IACUC-DWZX-2022–738).

CUMS paradigm

Eight–week CUMS procedures were carried out to induce cognitive deficits in the mice according to a previous protocol [22]. During CUMS, the mice were subjected to two different randomly chosen stressors to prevent habituation, including water and food deprivation for 24 h, cage tilting at 45° for 24 h, wet bedding for 12 h, physical restriction for 8 h, forced swimming for 2 min at 4 °C, shaking at 120 rpm for 30 min and inversion with a 12–h light/12–h dark cycle.

Cell culture

The human brain microvascular endothelial cell line hCMEC/D3 (ATCC, USA) preserves the in vivo endothelial phenotype [23]. The cells were maintained in EndoGRO–MV Complete Culture Medium (SCME004, Millipore) containing 0.2% EndoGRO–LS Supplement, 5 ng/mL recombinant human endothelial growth factor, 10 mM L–glutamine, 1 μg/mL hydrocortisone hemisuccinate, 0.75 U/mL heparin sulfate, 50 μg/mL ascorbic acid, 5% fetal bovine serum (FBS) and 1 ng/mL basic fibroblast growth factor in a humidified incubator at 37 °C containing 5% CO_2.

Rutin treatment

For in vivo treatment, rutin was dissolved in 0.5% sodium carboxymethyl cellulose (CMC–Na) to 5 mg/ml. After being subjected to the CUMS procedure for 6 weeks, all the mice received daily intragastric administration of rutin (100 mg/kg) or vehicle (0.5% CMC–Na) for 14 consecutive days. After the last administration, the behavioral tests were performed, and the mice were sacrificed. For in vitro treatment, rutin was dissolved in DMSO and diluted with sterile phosphate–buffered saline (PBS) to

the indicated concentrations. The cells were collected for further analysis following 12–48 h of treatment.

Cell proliferation assay

Cell proliferative activity was evaluated via the CCK8 method as described previously [24]. Briefly, cells were grown at a density of 5×10^3 cells per well on 96–well plates and cultured with 100 μM glucocorticoid (GC) or 12.5, 25 or 50 μM rutin or vehicle. At the indicated time points (0, 24 and 48 h), the cells were incubated with the 10 μl CCK8 reagent for 1 h at 37 °C. The OD value of the supernatant was measured at 450 nm with a microplate reader.

Transwell assay

The cell migratory capacity was determined via a transwell assay. Briefly, 1×10^4 cells were seeded into the upper chamber of a 8 μm polycarbonate transwell filter without FBS, and DMEM containing 10% FBS was added to the bottom chamber. After 24 h, the nonmigratory cells were removed with cotton swabs, and the invading cells were fixed with formalin for 20 min and dyed with 0.1% crystal violet for 15 min. Images were acquired via a microscope and analyzed via Image–Pro Plus software.

Wound healing assay

The cells were seeded in a 6–well plate at a density of 5×10^5 cells per well and cultured to 90% confluency. 200 μl pipette tips were used to generate three horizontal scratches in each well, which were subsequently washed with PBS to remove cell debris. The cells were subsequently incubated with 100 μM GC or 12.5, 25 or 50 μM rutin or vehicle. Finally, the distances of the wound boundaries at 0 (D_0), 12 (D_{12}) and 24 h (D_{20}) were measured, and the travelled distance percentage was determined as $(D_{0-}\ D_{12/24})/D_0\times100\%$.

Tube formation assay

The angiogenic effect of rutin was assessed via a tube formation assay as previously reported [25]. The cells were seeded in 96–well plates coated with Matrigel (354230, Corning) at a density of 2×10^4 cells per well and incubated at 37 °C for 24 h. Tube formation images were captured with an inverted microscope, and the numbers of tubes were analyzed via Image–Pro Plus software.

Assessment of hCMEC/D3 integrity

The transendothelial electrical resistance (TEER) across cellular monolayers was measured as previously described [26]. The cells (2×10^5 cells per well) were cultured on 12–well transwell inserts coated with rat tail collagen type I. After a monolayer was formed, cells were incubated with 100 μM GC or 12.5, 25 or 50 μM rutin or vehicle, and the EndOhm ohmmeter with chopstick electrodes was used to measure TEER. The TEER values ($\Omega.cm^2$) of cells were obtained by subtracting the TEER of the blank insert and multiplying by the surface area of the membrane for calculation. For the paracellular permeability of endothelial cell monolayers, 10 μM NaFI was added into the upper chambers and incubated for 1 h in 37 °C after treatment with GC and rutin. Then, 100 μl medium in the bottom chambers were collected and the content of NaFI in a microplate reader at 480 nm excitation and 538 nm emission wavelengths.

RNA–seq and data analysis

RNA–seq and data analysis were performed by Novogene (Beijing, China). Total RNA was extracted from hCMEC/D3 cells following incubation with rutin for 24 h via TRIzol reagent, and high–quality samples were selected using Bioanalyzer 2100 (Agilent Technologies, USA) for further analysis (RNA integrity number > 9, 260/280 ≈ 2.1). 3 μg of total RNA was used to construct sequencing RNA libraries using Rneasy Mini Plus Kit (Qiagen) and SMARTER mRNA–Seq Library Prep Kit, and the library was checked using Qubit 4.0 (Life Technologies, Waltham, USA) and Bioanalyzer 2100. The sequencing was then performed on the Illumina NovaSeq 6000 platform. Raw reads were firstly processed through FASTX–Toolkit software to obtain the clean data with high quality. Paired–end clean reads were aligned to the reference human genome (hg38) using Hisat2 software, and the numbers of reads mapped to each gene were counted using FeatureCounts software. DESeq2 R package software was applied to analyze differential expression between two groups. A corrected p value ≤ 0.05 or $|\log_2(\text{fold change})| \geq 1$ was set as the threshold for significantly differential expression. Gene Ontology (GO) analysis was used to classify the differentially expressed genes (DEGs) by the ClusterProfiler R package. GO terms were regarded as significantly enriched by differentially expressed genes when the corrected p value < 0.05.

Pharmacological treatment with pyroxamide

The mice were anesthetized with 1% isoflurane (v/v) and implanted with an indwelling cannula in the bilateral hippocampus via the following flat skull coordinates: − 2.2 mm caudal to the bregma, ± 1.9 mm from the midline, and − 1.9 mm deep from the skull. The cannula was secured to the skull with a stainless–steel screw and dental cement. After 6 weeks of CUMS procedures, 0.5 μl of pyroxamide (20 μM) per side was infused over 5 min, followed by 5 additional min to allow diffusion before withdrawal, and the injection was performed for 14 consecutive days.

Morris water maze (MWM)

The MWM apparatus was used to test the spatial learning and memory performance of the mice as previously described [27, 28]. Briefly, the maze was divided into four quadrants filled with opacified water, and the platform was placed 1 cm beneath the water surface in the center of one quadrant. For the navigation test, the mice were allowed to swim freely for 60 s. If the mice could not find the platform within 60 s, they were guided to the platform and allowed to stay there for 30 s. The probe trial was performed 24 h after the navigation test. The platform was removed, and the mice were allowed to pool for 60 s. The swimming activity of each mouse was recorded with a digital camera via the computer software of Water Maze.

Novel object recognition test (NORT)

The mice were allowed to habituate to the empty test apparatus 1 day before the experiment. In the training session, the mice were placed individually into the test apparatus containing two identical objects and allowed to explore freely for 10 min. One hour later, the mice were placed again for 10 min in the test chamber containing one familiar object and one novel object. The cognitive index was calculated according to the following formula: cognitive index = exploration time for novel object exploration/total exploration time during the test session × 100%.

Magnetic–activated cell sorting (MACS) of $CD31^+$ BMECs

The mouse hippocampus was harvested and digested into a single–cell suspension using Adult Brain Dissociation Kit (130107677, Miltenyi Biotec) by a gentleMACS Dissociator. The single-cell suspension was incubated with CD45 microbeads (10 µl per 1×10^7 cells) for 15 min at 4 °C and centrifuged at 300 g for 5 min. Then, the $CD45^-$fraction was collected and incubated with CD31 microbeads (10 µl per 1×10^7 cells) for 15 min at 4 °C. After centrifugation at 300 g for 5 min, the BMECs were isolated as $CD45^-$ $CD31^+$ cells using a MACS Separator.

Quantitative real–time PCR (qRT–PCR)

Total RNA from the cells or tissues was isolated with TRIzol reagent (#93,289, Sigma–Aldrich). Then, 2 µg RNA was used for the synthesis of cDNA via RT Master Mix (G490, Abmart) and SYBR–Green–based qPCR was conducted to evaluate the relative expression of the target genes using a LightCycler 96 Realtime PCR System (Roche, Switzerland). The relative levels of the target genes were calculated by $2^{-\Delta\Delta Ct}$ method. The sequences of the primers used are shown in Table S1.

Western blotting

Brain capillaries were extracted according to Menard et al. [1] with minor modifications. The bilateral hippocampus of 6–7 mice were homogenized in 1 mL of cold DMEM. The homogenate was centrifuged at 4000 g for 5 min at 4 °C and the pellet was resuspended in the 18% dextran solution followed by centrifugation at 6000 g for 10 min at 4 °C. The pellet obtained was then resuspended in DMEM containing 1 mg/mL collagenase/dispase, 40 µg/mL DNase 1 and 0.147 µg/mL tosyllysine chloromethyl ketone. The mixture was incubated at 37 °C for 75 min and centrifuged at 4000 g for 10 min at room temperature to collect the capillary extracts. Capillary extracts and cell samples were then lysed in RIPA lysis buffer (C1053+, Applygen) supplemented with protease inhibitor cocktail (B14001, Bimake). The cell lysates were cleared by centrifugation at 12,000 rpm at 4 °C for 15 min, and the protein concentration was quantified via a bicinchoninic acid (BCA) assay. Each sample containing 20 µg of protein was denatured, loaded onto a 10–12.5% SDS–polyacrylamide gel for electrophoresis, and then transferred onto polyvinylidene difluoride (PVDF) membranes. The membranes were incubated in 5% nonfat milk for 1 h at room temperature and probed with the following antibodies at 4 °C: Claudin–5 (1:500, 35–2500, Thermo Fisher Scientific,), HDAC1 (1:1000, #34,589, CST), H3K27ac (1:1000, A7253, ABclonal), C/EBPα (1:1000, #8178, CST), β–actin (1:50,000, AC038, ABclonal) and GAPDH (1:50,000, AC19056, ABclonal). After being washed in TBST for 3 × 10 min, the membranes were incubated with the following secondary antibodies for 2 h at room temperature: goat anti–mouse IgG (H + L) (1:5000, ZB–5305, ZSGB–BIO) and goat anti–rabbit IgG (H + L) (1:5000, ZB–5301, ZSGB–BIO). The membranes were visualized with enhanced chemiluminescence, and the band intensities were quantified via ImageJ. The relative expression of the target proteins was normalized to the β–actin level on the same blot.

Immunofluorescence

Immunostaining was performed according to Menard et al. [29]. The mouse brains were quickly frozen in Tissue–Tek O.C.T. compound (#4583, SAKURA) on dry ice, and sectioned at 15 µm. The sections were fixed in methanol for 10 min at − 20 °C, blocked in PBS containing 0.1%

Triton X–100 and 3% bovine serum albumin (BSA) and incubated with primary antibodies against CD31 (1:100, #5550274, BD Biosciences), Claudin–5 (1:100, 35–2500, Thermo Fisher Scientific), HDAC1 (1:200, #34589, CST) and H3K27ac (1:200, A7253, ABclonal) at 4 °C overnight. The sections were then rinsed with PBS and incubated with appropriate secondary antibodies (Cy3 AffiniPure donkey anti–mouse IgG (H + L), 1:200, 715–165–151, Jackson; Alexa Fluor 488 AffiniPure donkey anti–mouse IgG (H + L), 1:200, 715–545–150, Jackson; Cy3 AffiniPure donkey anti–rabbit IgG (H + L), 1:200, 711–165–152, Jackson; Cy3 goat anti-rat IgG (H + L), A10522, Thermo Fisher Scientific; Oregon Green–488 conjugate of NeutrAvidin biotin-binding protein, A6374, Thermo Fisher Scientific). The sections were stained with Hoechst (1:500, C0031, Solarbio), and images were acquired via a confocal laser–scanning microscope (Leica TCS SP8 STED). Cells exhibiting specific Claudin–5 fluorescence signals accompanied by clearly visible nuclear were defined as Claudin–5 positive regions and subjected to quantification using Image–Pro Plus software.

Chromatin immunoprecipitation (ChIP)

ChIP was performed according to the instructions of the SimpleChIP® Plus Enzymatic Chromatin IP Kit (#9005, CST). Dissected mouse hippocampus or cultured hCMEC/D3 cells were cross–linked with 1.5% formaldehyde for 20 min at room temperature and glycine was then added to stop cross–linking. The samples were centrifuged at 500 g for 5 min at 4 °C and the collected pellets were disaggregated into a single–cell suspension using a Dounce homogenizer. Chromatin fragments of 150–900 bp were subsequently generated via incubation with micrococcal nuclease (0.5 µl per 4×10^6 cells or per 25 mg tissue) for 20 min. Next, the samples were incubated with antibodies against H3K27ac (1:100, A7253, ABclonal), HDAC1 (1:100, ab280198, Abcam) and C/EBPα (1:100, #8178, CST) overnight at 4 °C followed by incubation with ChIP–grade Protein G magnetic beads for 2 h at 4 °C. The DNA was purified for qPCR analysis after the reversal of protein–DNA cross–linking. The primers used for ChIP–qPCR were listed in Table S2.

Enzyme–linked immunosorbent assay (ELISA)

The levels of TNF–α in the blood and hippocampus of the mice were determined via a solid–phase sandwich TNF–α ELISA kit (D721217, Sangon Biotech) according to the manufacturer's protocols. Briefly, 100 µl of the standard working solution or samples was added to each well of reaction plates and incubated for 90 min at 37 °C. Then, 100 µl of biotin-labeled TNF-α antibody working solution was added to each well and incubated for 60 min at 37 °C. Each well was soaked with 350 µl of washing buffer for 4 times and incubated with 100 µl of HRP-labeled streptavidin working solution for 30 min at 37 °C. Finally, 90 µl of chromogenic reagent was added to each well for 15 min at 37 °C in the dark. The absorbance of each sample was measured at 450 nm via a Spectra microplate reader.

BBB permeability measurement

Mouse BBB permeability was assessed as previously described [30]. The mice were given 10 mg of sodium fluorescein (NaFI) or fluorescein isothiocyanate (FITC)–dextran and permitted to circulate for 1 h. Blood serum was collected, and the hippocampus was then isolated following transcardial perfusion with 0.9% saline. The hippocampus was subsequently homogenized in a 1:1 volume of 2% trichloroacetic acid and centrifuged at 3000 rpm for 10 min. The supernatants were mixed with 0.05 M borate buffer at a ratio of 1:1, and the fluorescence was measured in 100 µl of the mixture via a microplate reader (excitation at 480 nm, emission at 538 nm). BBB permeability was calculated as the ratio of the brain region fluorescence intensity to the serum fluorescence intensity and is presented as the fold increase compared with the permeability in non–stressed control mice.

Transmission electron microscopy (TEM)

TEM was used for the morphological examination of the TJ structures. The mouse hippocampus was fixed in 2.5% glutaraldehyde for 2 h at 4 °C and washed in 0.1 M phosphate buffer. The samples were subsequently postfixed in 1% osmium tetroxide/0.1 M cacodylate buffer and dehydrated through a graduated ethanol to propylene oxide series followed by resin infiltration polymerization at 60 °C for 48 h. Ultrathin sections (60–80 nm) were counterstained with uranyl acetate and lead citrate, and the samples were detected via electron microscopy.

Statistical analysis

All the data are presented as the means ± standard errors of the means (SEM), and the statistical analysis was conducted via GraphPad Prism 9.0 software. Normality assumptions were evaluated via the D'Agostino–Pearson omnibus normality test, and nonparametric tests were used for the data that failed the test. Two groups were compared via a two–tailed Student's *t* test following a normal distribution. Comparisons among three or more groups were performed by one–way ANOVA, followed by Tukey's multiple comparisons test or two–way ANOVA, followed

by Bonferroni post hoc correction. The samples, sizes, statistical tests, and statistical results are indicated in the corresponding figure legends. Significance was determined as $p < 0.05$.

Results

Rutin alleviates stress–induced cognitive impairments and BBB breakdown in mice

To investigate the effects of rutin on the cognitive deficits induced by chronic stress, we evaluated the behavioral performance of the mice through the NORT and MWM. The oral administration of rutin increased the cognitive index in the NORT of CUMS mice ($F_{(2,18)} = 6.814$, $p = 0.0063$; Fig. 1A, B). Moreover, the CUMS + Rutin mice displayed reversion of spatial learning and memory deficits, as reflected by a shorter escape latency to the target quadrant, more target entries and more time spent in the target quadrant than the CUMS mice did (escape latency during the training trial: $F_{(10,90)} = 5.740$, $p < 0.0001$; escape latency during the probe trial: $F_{(2,\ 18)} = 14.12$, $p = 0.0002$; target entries: $F_{(2,18)} = 7.032$, $p = 0.0055$; time spent in target quadrants: $F_{(2,18)} = 9.338$, $p = 0.0017$; Fig. 1C–F, Fig. S1A). Moreover, there were no significant differences in the mean swimming speed among the mice (Fig. S1B), suggesting that the improvements in these phenotypes in the CUMS + Rutin mice did not result from altered motor function.

The involvement of BBB disruption in the development of cognitive impairment has been increasingly confirmed [31, 32]. Considering the protective role of rutin in vascular barrier function [33, 34], we examined its effect on BBB integrity under stressful circumstances. The TEM analysis revealed that rutin rescued the morphological abnormalities of the hippocampal capillaries characterized by increased discontinuous TJs in the CUMS model mice ($F_{(2,6)} = 68.52$, $p < 0.0001$; Fig. 1G, H). We next compared BBB integrity in Ctrl, CUMS and CUMS + Rutin mice via two types of fluorescent dyes (NaFI and FITC–Dextran) individually. High infiltrations of both NaFI and FITC–dextran dyes were observed in the hippocampus of CUMS but not Ctrl or CUMS + Rutin mice (NaFI: $F_{(2,9)} = 20.9$, $p = 0.0004$; FITC–Dextran: $F_{(2,9)} = 34.5$, $p < 0.0001$; Fig. 1I, J), suggesting that rutin could prevent BBB breakdown in these mice. Together, these results indicate that rutin treatment significantly ameliorates learning and memory deficits and BBB damage induced by chronic stress.

Rutin facilitates the integrity of hCMEC/D3 cells

Given that BMECs are the major functional constituents of the BBB, it is tempting to hypothesize that rutin alleviates BBB breakdown by modifying BMEC function. To validate this hypothesis, the stress hormone GC was applied to hCMEC/D3 cells to construct an in vitro model of chronic stress as previously reported [35, 36], and the role of rutin in endothelial cell proliferation was investigated. The CCK8 assay indicated that GC inhibited the proliferation of hCMEC/D3 cells following 24 and 48 h of treatment, whereas rutin at 12.5–50 μM reversed this phenomenon within a certain concentration range (24 h: $F_{(4,15)} = 5.186$, $p = 0079$; 48 h: $F_{(4,15)} = 10.85$, $p = 0002$; Fig. 2A). We also performed a wound healing assay and a transwell assay to examine the migration capacity of endothelial cells. The percentage of distance traveled by the cells incubated with rutin was greater than that traveled by the GC group (12 h: $F_{(4,15)} = 24.82$, $p < 0.0001$; 24 h: $F_{(4,15)} = 65.29$, $p < 0.0001$; Fig. 2B, C). Consistently, the transwell assay results revealed that the numbers of migrated hCMEC/D3 cells increased upon rutin treatment ($F_{(4,15)} = 101.4$, $p < 0.0001$; Fig. 2D, E). These findings reveal that rutin antagonizes the inhibitory effect of stress on endothelial cell proliferation and migration. Angiogenesis is another major intrinsic property of BMECs. In the tube formation assay, rutin–incubated hCMEC/D3 cells exhibited greater angiogenetic ability than the GC group did ($F_{(4,15)} = 31.75$, $p < 0.0001$; Fig. 2F, G). Further, rutin could enhance barriers properties of hCMEC/D3 cells characterized by the increased TEER value and the reduced permeability to NaFI (TEER: $F_{(4,15)} = 8.234$, $p = 0.0010$; NaFI flux: $F_{(4,15)} = 10.93$, $p = 0.0002$; Fig. 2H, I). Collectively, these results indicate that rutin treatment enhances the function of BMECs.

(See figure on next page.)

Fig. 1 Rutin ameliorates cognitive and BBB deficits in CUMS mice. **A** Experimental timeline of the CUMS procedure and rutin treatment in mice. **B** Cognitive index of Ctrl, CUMS and CUMS with rutin treatment (CUMS + Ru) mice in the NORT (One–way ANOVA with Tukey's post hoc test, n = 7 mice for each group). **C** Escape latency to reach the platform of the mice during the training trials in the MWM (One–way ANOVA with Tukey's post hoc test, n = 7 mice for each group). **D**–**F** Escape latency (**D**), target entries (**E**) and time spent in the target quadrant (**F**) by the mice in the probe trial of the MWM (One–way ANOVA with Tukey's post hoc test, n = 7 mice for each group). **G** Representative TEM images of TJ structure in Ctrl, CUMS and CUMS + Ru mice. Scale bar, 500 nm (white arrowheads: intact TJs; red arrowheads: discontinuous TJs). **H** Quantification of the percentages of discontinuous TJs in the (**G**) (One–way ANOVA with Tukey's post hoc test, n = 3 mice for each group, 50–60 TJs per mouse). **I**, **J** Hippocampal permeability of the BBB to NaFI (**I**) and FITC–Dextran (**J**) in the mice (One–way ANOVA with Tukey's post hoc test, n = 4 mice for each group). The data are presented as the mean ± SEM. $^{**}p < 0.01$, $^{***}p < 0.001$, vs Ctrl; $^{\#}p < 0.05$, $^{\#\#}p < 0.01$, $^{\#\#\#}p < 0.001$, vs CUMS

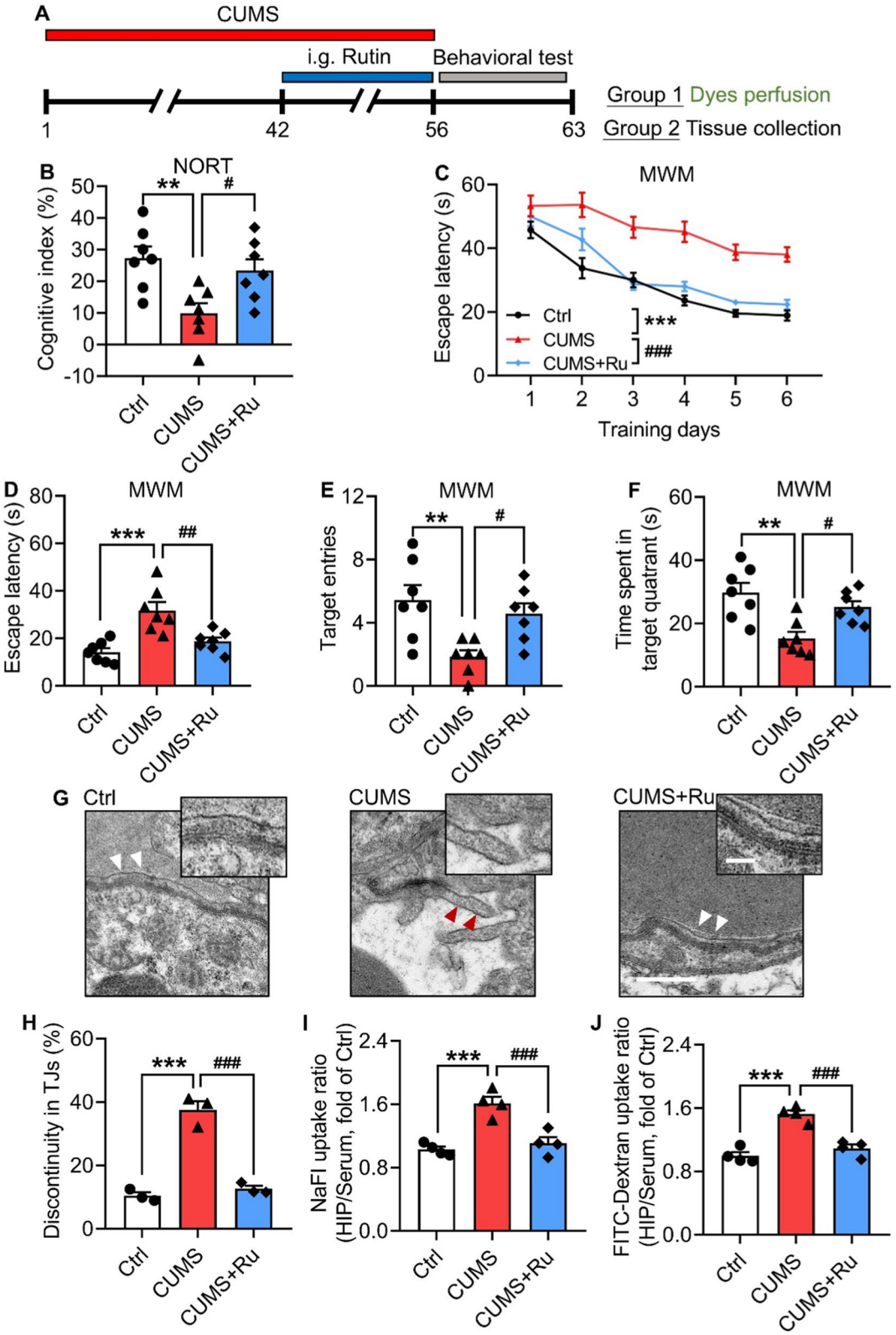

Fig. 1 (See legend on previous page.)

Genome–wide identification of target genes of rutin in hCMEC/D3 cells

To decipher the molecular mechanisms by which rutin regulates BMEC function and BBB integrity, we performed high–throughput RNA–seq analysis in hCMEC/D3 cells. Compared with those in the DMSO group, 6430 DEGs were identified in the rutin–treated hCMEC/D3 cells, of which 3407 were upregulated and 3023 were downregulated (Fig. 3A, B). The main functions of these DEGs were classified via GO pathway analysis. The results suggested that the rutin–targeting genes were involved in 65 significant biological processes including cell junction organization, cell migration and proliferation, and histone modification (Fig. 3C). To verify the RNA–seq results at the individual gene level, we performed qRT–PCR on selected genes, including *CLDN5, MACF1, PRKDC, SPHK1, CYBA, VEGFB, HDAC1 and TADA3*, which represent each of the representative classified pathways of the GO analysis. The changes in the mRNA levels of these genes were consistent with the findings of the RNA–seq data (*CLDN5*: $t_4 = 9.816$, $p = 0.006$; *MACF1*: $t_4 = 20.34$, $p < 0.0001$; *PRKDC*: $t_4 = 13.11$, $p = 0.0002$; *SPHK1*: $t_4 = 17.37$, $p < 0.0001$; *CYBA*: $t_4 = 15.65$, $p < 0.0001$; *VEGFB*: $t_4 = 7.122$, $p = 0.0021$; *HDAC1*: $t_4 = 4.864$, $p = 0.0083$; *TADA3*: $t_4 = 11.11$, $p = 0.0004$; Fig. 3D). These results indicate that rutin administration facilitates the expression of genes some of which are involved in endothelial cell proliferation, cell junctions and epigenetic regulation.

Rutin promotes H3K27ac recruitment at the *Cldn5* promoter to restore its expression in CUMS mice

Notably, *Cldn5* (the gene encoding the protein Claudin–5), a dominant regulator of BBB integrity [8], was identified as a target gene of rutin via RNA–seq analysis. We confirmed a specific reduction in the Claudin–5 protein level in the hippocampus, which was reversed by rutin treatment under stressful conditions (Claudin–5/β–actin: $F_{(2,9)} = 31.72$, $p < 0.0001$; Fig. 4A, B). Next, we explored the underlying mechanism by which rutin restores Claudin–5 expression. Previous studies have revealed that aberrant histone modifications such as H3K27me3 and H3K27ac result in *Cldn5* transcriptional repression [37–39], and our RNA–seq data also suggested that rutin–targeting genes were enriched in histone modification pathways (Fig. 3C). Therefore, we propose that rutin regulates the epigenetic signature to drive beneficial changes in Claudin–5. Rutin strengthened endothelial permissive H3K27ac modification in the hippocampus of CUMS mice, whereas rutin failed to alter repressive H3K27me3 deposition (H3K27ac/β–actin: $F_{(2,9)} = 9.821$, $p = 0.0128$; H3K27ac labeling intensity: $F_{(2,6)} = 7.669$, $p = 0.0222$; Fig. 4C, D; Fig. S2; Fig. S3A and B). Moreover, in line with the RNA–seq data, the expression of HDAC1, which is the deacetylase of H3K27ac, was also reduced by rutin treatment in the hippocampal BMECs of stressed mice, whereas other H3K27ac modification enzymes, including HDAC2 and EP300, showed no obvious changes (*Hdac1* mRNA: $F_{(2,9)} = 29.21$, $p = 0.0001$; HDAC1/β–actin: $F_{(2,9)} = 23.03$, $p = 0.0003$; HDAC1 labeling intensity: $F_{(2,6)} = 6.935$, $p = 0.0275$; Fig. 4E–G; Fig. S3C and D). We subsequently examined the content of *Cldn5* promoter–bound H3K27ac and HDAC1 via a ChIP assay. Compared with those in the Ctrl group, decreased H3K27ac and increased HDAC1 signals were observed 600 bp upstream from the transcription start site (TSS) of *Cldn5* in the CUMS group, while these phenotypes were abolished in the CUMS + Rutin group (H3K27ac enrichment: $F_{(2,6)} = 24.14$, $p = 0.0014$; HDAC1 enrichment: $F_{(2,6)} = 60.94$, $p = 0.0001$; Fig. 4H–J).

Additionally, to validate the causal role of increased HDAC1–dependent histone deacetylation in stress–induced *Cldn5* loss, the HDAC1 inhibitor pyroxamide or vehicle was also directly infused into the bilateral hippocampus through an implanted cannula for 14 consecutive days following the 6–week CUMS procedure (Fig. S4A). The administration of pyroxamide increased Claudin–5 expression in line with the rescue of H3K27ac loss (H3K27ac enrichment: $F_{(2,9)} = 26.87$, $p = 0.0002$; H3K27ac/β–actin: $F_{(2,6)} = 21.14$, $p = 0.0019$; Claudin–5/β–actin: $F_{(2,6)} = 28.86$, $p = 0.0008$; Fig. S4B–F). In the hCMEC/D3 cells, pyroxamide at doses of 10 and 20 μM enhanced the bound H3K27ac modification and increased Claudin–5 expression following

(See figure on next page.)

Fig. 2 Rutin promotes the integrity of cerebral microvascular endothelial cells. **A** Proliferation of rutin–treated hCMEC/D3 cells after 24 and 48 h determined by a CCK8 assay (One–way ANOVA with Tukey's post hoc test, n = 4 biological replicates). **B** Representative images of wound healing in rutin–treated cells at 0, 12 and 24 h. Scale bar: 200 μm. **C** Quantification of the distances traveled during wound healing in the (**B**) (One–way ANOVA with Tukey's post hoc test, n = 4 biological replicates). **D** Representative images of transwell assays in rutin–treated cells. Scale bar: 200 μm. **E** Quantification of the numbers of migrated cells in the (**D**) (One–way ANOVA with Tukey's post hoc test, n = 4 biological replicates). **F** Representative images of tube formation in rutin–treated cells. Scale bar, 50 μm. **G** Quantification of the tubes in the (**F**) (One–way ANOVA with Tukey's post hoc test, n = 4 biological replicates). **H** The TEER value of rutin-treated cells (One–way ANOVA with Tukey's post hoc test, n = 4 biological replicates). **I** The flux of NaFl in rutin-treated cells (One–way ANOVA with Tukey's post hoc test, n = 4 biological replicates). The data are presented as the mean ± SEM. $^{*}p < 0.05$, $^{**}p < 0.01$, $^{***}p < 0.001$, vs DMSO; $^{\#}p < 0.05$, $^{\#\#}p < 0.01$, $^{\#\#\#}p < 0.001$, vs GC

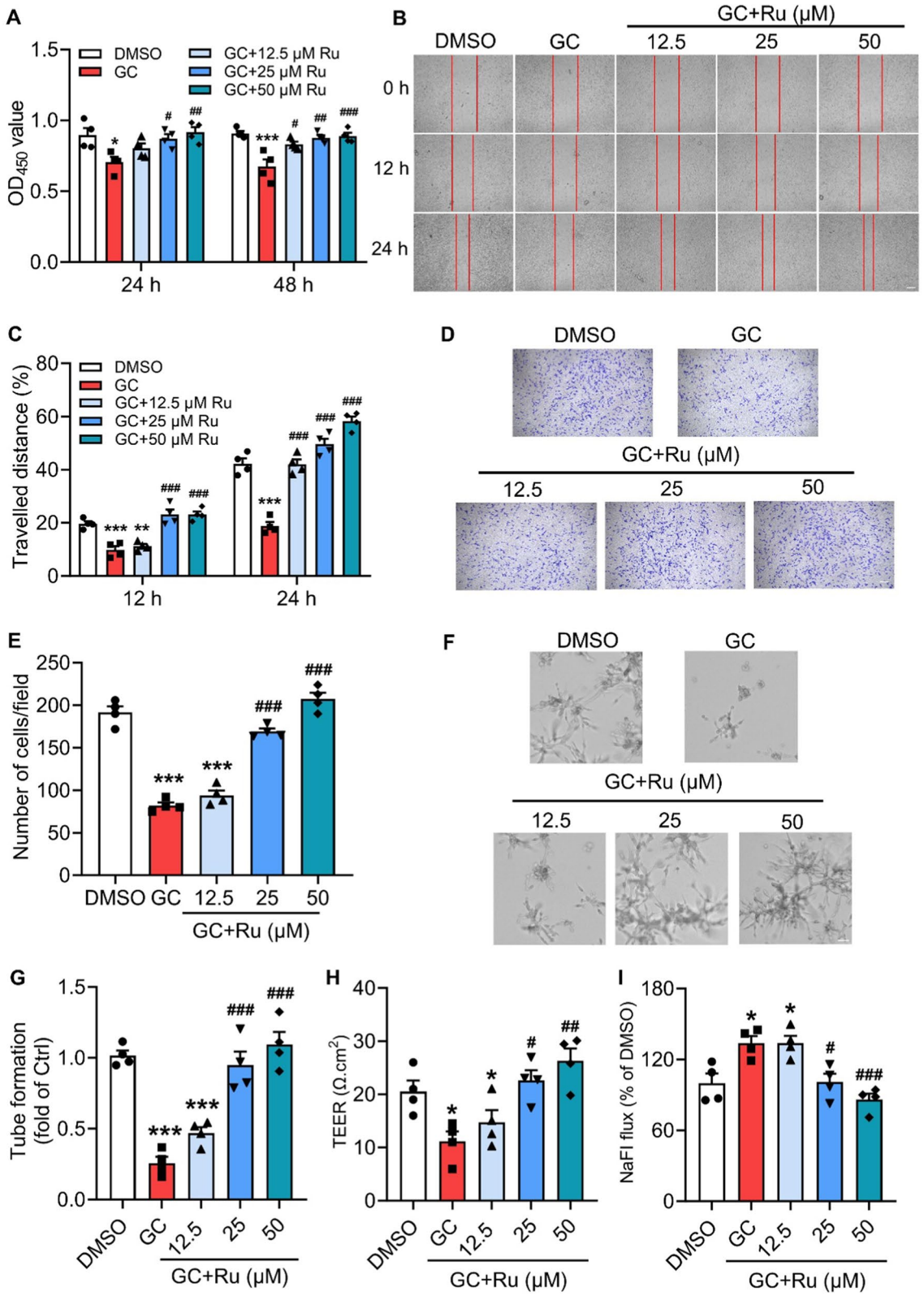

Fig. 2 (See legend on previous page.)

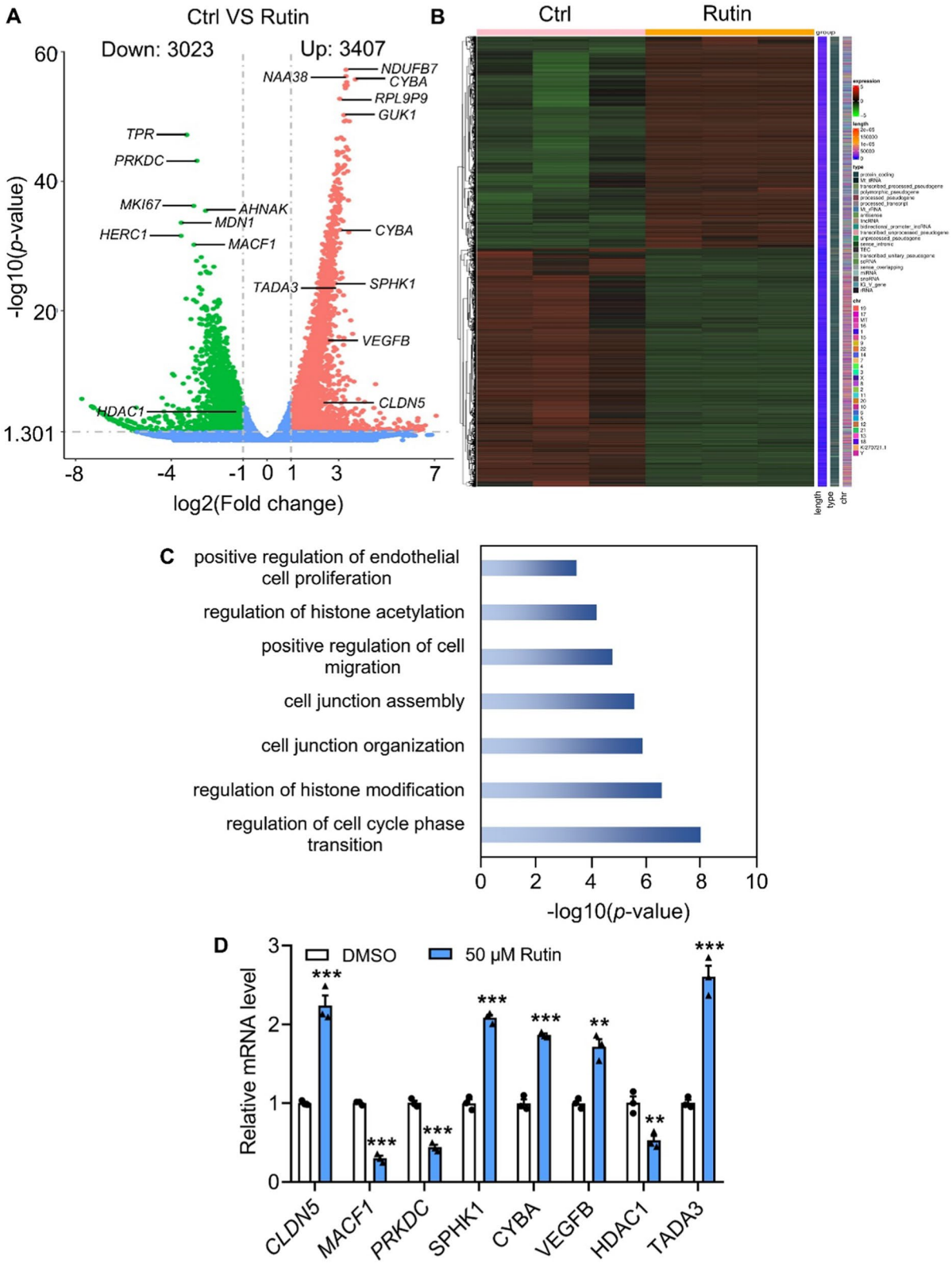

Fig. 3 Genome–wide identification of rutin-targeting genes in hCMEC/D3 cells via whole–transcriptome RNA sequencing. **A** Volcano plot of the DEGs in hCMEC/D3 cells with rutin treatment. **B** Heatmap of the DEGs in hCMEC/D3 cells with rutin treatment. **C** The biological process categories of the DEGs by GO analysis. **D** Representative DEG mRNA levels in rutin-treated hCMEC/D3 cells determined by RT-qPCR (One–way ANOVA with Tukey's post hoc test, n = 3 biological replicates). The data are presented as the mean ± SEM. $^{**}p < 0.01$, $^{***}p < 0.001$

24 h of incubation (H3K27ac enrichment: $F_{(2,9)}=34.59$, $p<0.0001$; H3K27ac/β–actin: $F_{(2,6)}=70.68$, $p<0.0001$; Claudin–5/β–actin: $F_{(2,6)}=34.23$, $p=0.0005$; Fig. S4G–K). Also, pyroxamide could increase the TEER value and inhibit the NaFI flux of the hCMEC/D3 cells (TEER: $F_{(2,9)}=18.88$, $p=0.0006$; NaFI flux: $F_{(4,15)}=7.281$, $p=0.0132$; Fig. S4L and M). These findings suggest that rutin prevents HDAC1 from binding to the *Cldn5* promoter to facilitate H3K27ac recruitment, contributing to the restoration of Claudin–5 expression.

Rutin induced *Cldn5* upregulation through the enhancement of C/EBPα transcriptional activity in CUMS mice

Having established that rutin can repair the epigenetic modification of *Cldn5*, we next investigated how rutin transcriptionally regulates *Cldn5* expression. C/EBPα has been identified as a transcription factor to evoke the expression of Claudin–5 [40, 41]. Consistent with previous studies, we found that C/EBPα knockdown inhibited Claudin–5 expression (C/EBPα/β–actin: $t_4=6.654$, $p=0.026$; Claudin–5/β–actin: $t_4=5.086$, $p=0.071$; Fig. S5). Although endothelial C/EBPα expression in the hippocampus remained unchanged among the different groups (Fig. 5A, B), rutin treatment remarkably stabilized the interaction of C/EBPα with the *Cldn5* promoter region where H3K27ac deposition was increased ($F_{(2,9)}=27.01$, $p=0.0002$; Fig. 5C, D). Additionally, we found that the interaction of C/EBPα with the *Cldn5* promoter was enhanced in the presence of pyroxamide in CUMS mice and hCMEC/D3 cells (CUMS mice: $F_{(2,9)}=23.09$, $p=0.0003$; hCMEC/D3 cells: $F_{(2,9)}=11.63$, $p=0.0032$; Fig. 5E, F). Together, the above data demonstrate that rutin restores *Cldn5* transcription through increasing C/EBPα binding to its promoter.

Rutin blocks the infiltration of circulating TNF–α into the brain of CUMS mice

The hyperpermeable BBB results in the leakage of peripheral proinflammatory cytokines into the central nervous system (CNS), contributing to the development of neurological diseases [29, 37]. TNF–α, a proinflammatory cytokine involved in stress vulnerability, has previously been reported to penetrate the compromised BBB of CUMS model mice [37]. Accordingly, we evaluated whether rutin could attenuate the CUMS–induced invasion of circulating TNF–α. We observed an intense increase in TNF–α in the plasma and hippocampus of CUMS model mice, which could be rescued by rutin treatment (serum: $F_{(2,15)}=24.08$, $p<0.0001$; hippocampus: $F_{(2,15)}=21.57$, $p<0.0001$; Fig. 6A, B). To determine whether rutin could restrain the ability of circulating TNF–α to penetrate the brain, we intravenously injected biotinylated recombinant TNF–α into the blood of Ctrl, CUMS and CUMS + Rutin mice and examined its abundance in the hippocampus via the Oregon Green–488 conjugate of NeutrAvidin biotin–binding protein (Fig. 6C). The hippocampus was largely permeable to circulating TNF–α under stressful conditions, whereas rutin replenishment prevented TNF–α aggregation around the blood vessels where Claudin–5 was downregulated (Fig. 6D, E). Together, these findings suggest that rutin treatment inhibits the direct passage of TNF–α through the damaged BBB, thus alleviating chronic stress–induced cognitive dysfunction.

Discussion

Our findings demonstrated that rutin boosted the ability of proliferation, migration and angiogenesis, and the monolayer integrity in BMECs. Moreover, rutin abrogated the recruitment of the histone deacetylase HDAC1 to the *Cldn5* promoter and stabilized permissive H3K27ac deposition, thereby activating Claudin–5 generation. Furthermore, the restorative effect of rutin treatment on BMEC function and *Cldn5* transcription reversed BBB damage, and blocked the passage of circulating TNF–α into the hippocampus parenchyma, which subsequently attenuated stress–induced cognitive deficits (Fig. 6F). Collectively, our results suggest that rutin is

(See figure on next page.)

Fig. 4 Rutin maintains H3K27ac modification to rescue Claudin–5 expression in CUMS mice. **A** Representative images of Claudin–5 protein levels in the hippocampus of mice as determined by western blotting. **B** Quantification of the Claudin–5 protein levels in the (**A**) (One–way ANOVA with Tukey's post hoc test, n = 4 biological replicates). **C** Representative images of H3K27ac protein levels in the hippocampus of Ctrl, CUMS and CUMS + Ru mice by western blotting. **D** Quantification of the H3K27ac protein levels in the (**C**) (One–way ANOVA with Tukey's post hoc test, n = 4 biological replicates). **E** *Hdac1*, *Hdac2* and *Ep300* mRNA levels in the hippocampus of the mice (One–way ANOVA with Tukey's post hoc test, n = 4 biological replicates). **F** Representative images of HDAC1 protein levels in the hippocampus of mice by western blotting. **G** Quantification of the HDAC1 protein levels in the (**F**) (One–way ANOVA with Tukey's post hoc test, n = 4 biological replicates). **H** Diagram of the designed primer pairs for the indicated regions. **I** Enrichment of H3K27ac modifications at different sites of the *Cldn5* promoter in the hippocampus of mice (One–way ANOVA with Tukey's post hoc test, n = 3 biological replicates). **J** Enrichment of HDAC1 600 bp upstream from the *Cldn5* TSS in the hippocampus of mice (One–way ANOVA with Tukey's post hoc test, n = 3 biological replicates). The data are presented as the mean ± SEM. $^{*}p<0.05$, $^{***}p<0.001$, vs Ctrl; $^{\#}p<0.05$, $^{\#\#}p<0.01$, $^{\#\#\#}p<0.001$, vs CUMS

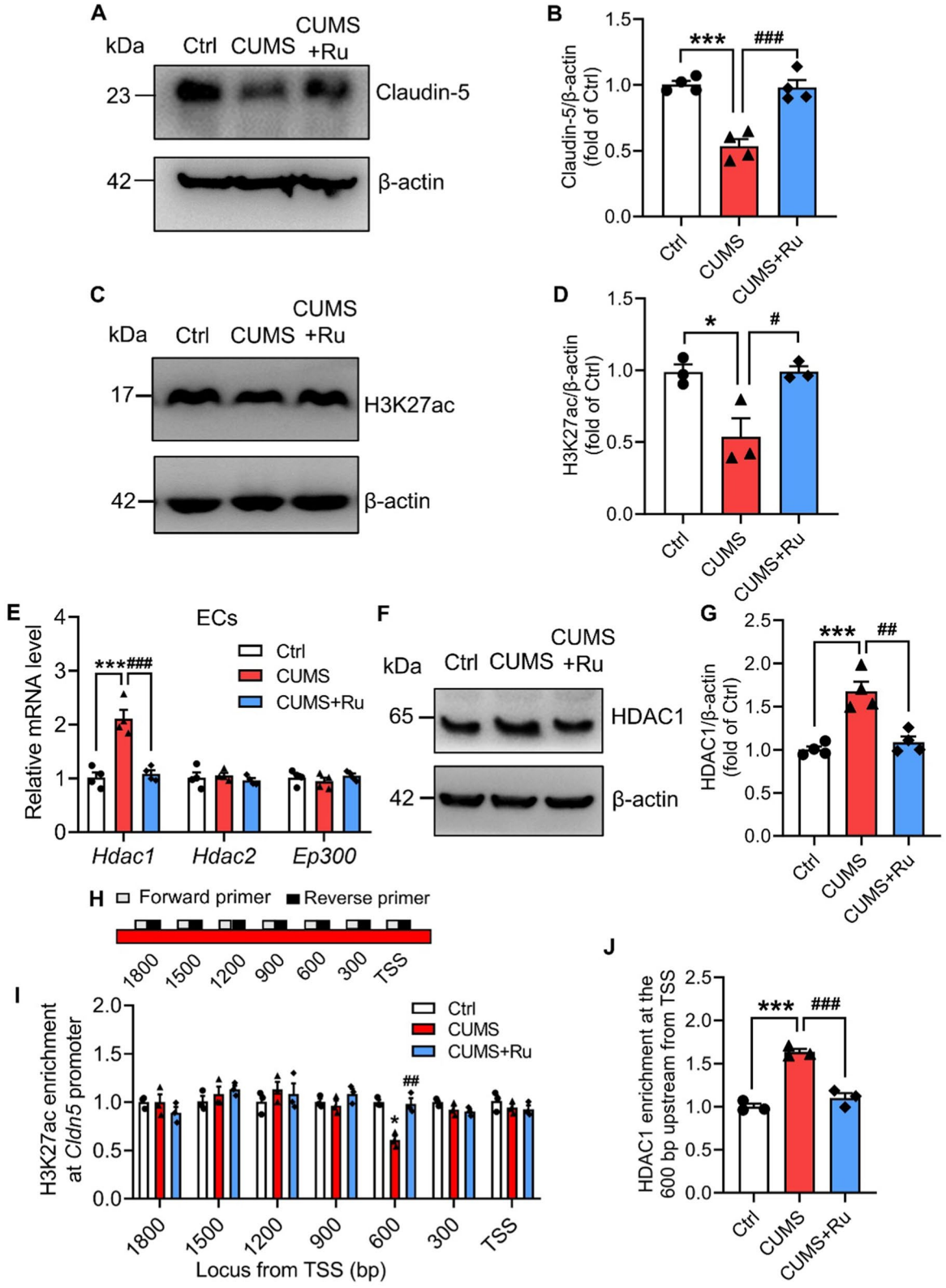

Fig. 4 (See legend on previous page.)

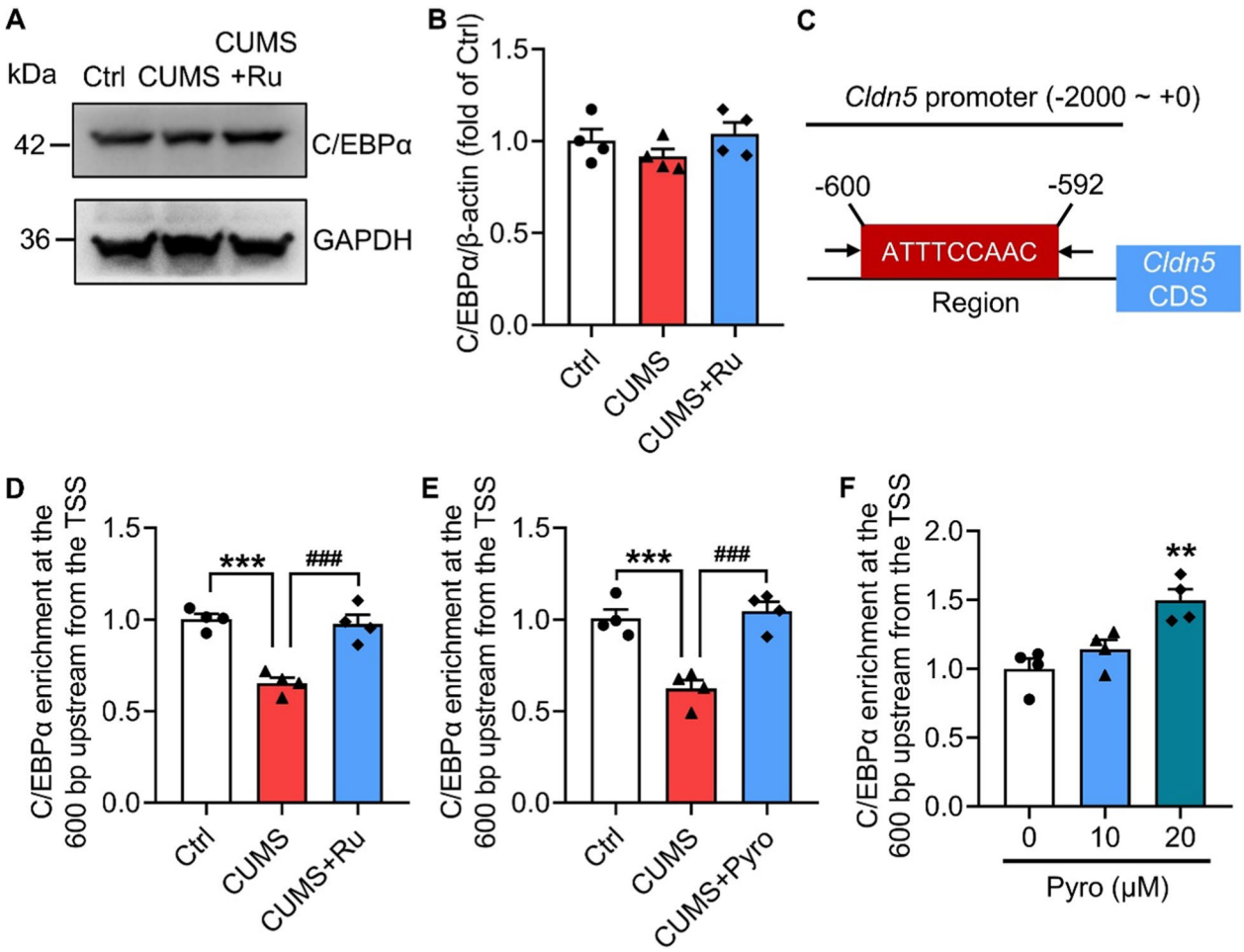

Fig. 5 Rutin enhances the binding of C/EBPα to the *Cldn5* promoter in CUMS mice. **A** Representative images of C/EBPα protein levels in the hippocampus of Ctrl, CUMS and CUMS + Ru mice by western blotting. **B** Quantification of the C/EBPα protein levels in the (**A**) (One–way ANOVA with Tukey's post hoc test, n = 4 biological replicates). **C** Diagram of the predicted binding site of C/EBPα to the *Cldn5* promoter. **D** Enrichment of C/EBPα 600 bp upstream from the *Cldn5* TSS in the hippocampus of mice (One–way ANOVA with Tukey's post hoc test, n = 4 biological replicates). **E** Enrichment of C/EBPα 600 bp upstream from the *Cldn5* TSS in CUMS mice with pyroxamide (Pyro) treatment (One–way ANOVA with Tukey's post hoc test, n = 4 biological replicates). **F** Enrichment of C/EBPα 600 bp upstream from the *Cldn5* TSS in hCMEC/D3 cells treated with 0, 10 and 20 μM Pyro (One–way ANOVA with Tukey's post hoc test, n = 4 biological replicates). The data are presented as the mean ± SEM. $^{*}p < 0.05$, $^{**}p < 0.01$, $^{***}p < 0.001$, vs Ctrl; $^{\#\#\#}p < 0.001$, vs CUMS

a promising drug candidate for stress–induced cognitive impairments by targeting crucial components of the BBB.

Despite its poor water solubility and low bioavailability, rutin is able to cross the BBB to exert multiple neuroprotective effects [15, 18]. Rutin prevents the microglial synapse engulfment and the neuronal synapse loss by the normalization of NF–κB pathway and the reduction of tau pathology in AD mouse models [14].

(See figure on next page.)

Fig. 6 Rutin inhibits the passage of circulating TNF–α into the hippocampus of CUMS mice. **A**, **B** TNF–α protein levels in the blood (**A**) and hippocampus (**B**) of Ctrl, CUMS and CUMS + Ru mice (One–way ANOVA with Tukey's post hoc test, n = 6 mice for each group). **C** Experimental timeline of CUMS, rutin treatment and biotinylated TNF–α detection. **D** Representative images of DAPI (blue), biotinylated TNF–α (green) and Claudin–5 (red) immunostaining in the hippocampus of Ctrl, CUMS and CUMS + Ru mice. Scale bar, 2 μm. **E** Representative images of DAPI (blue), biotinylated TNF–α (green) and CD31 (red) immunostaining in the hippocampus of Ctrl, CUMS and CUMS + Ru mice. Scale bar, 2 μm. **F** Schematic showing that rutin treatment promoted endothelial cell proliferation, migration and angiogenesis. Moreover, rutin inhibited HDAC1–dependent H3K27 deacetylation to facilitate the transcriptional activity of C/EBPα at the *Cldn5* promoter. As a result, rutin reversed chronic stress–induced *Cldn5* loss and BBB breakdown. Furthermore, the restoration of rutin on the BBB blocked the infiltration of circulating TNF–α into the hippocampus and attenuated cognitive dysfunction. The data are presented as the mean ± SEM. $^{***}p < 0.001$, vs Ctrl; $^{\#\#\#}p < 0.001$, vs CUMS

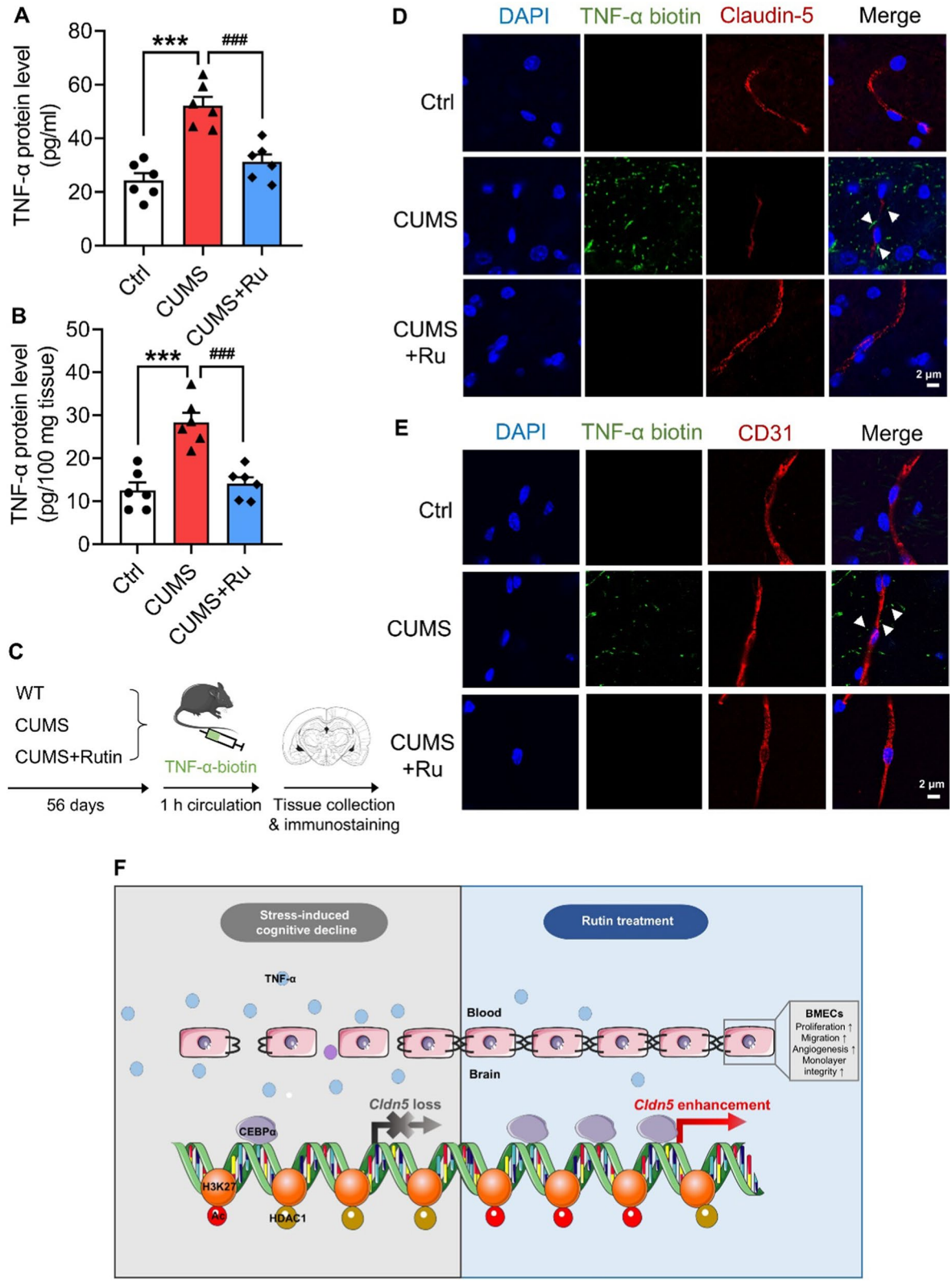

Fig. 6 (See legend on previous page.)

The inhibitory effect of rutin on Aβ oligomer level and neuronal apoptosis also contribute to the cognitive disturbances [42, 43]. Additionally, rutin can suppress the release of pro–inflammatory cytokines such as TNF–α and IL–6, and reverse the oxidative stress characterized by low antioxidants and lipid peroxidation in discrete brain regions, thus ameliorating learning and memory impairments [44, 45]. In our current study, oral administration of rutin successfully rescued the CUMS–induced cognitive decline as observed in the form of memory via repairing neurovascular dysfunction.

BBB dysfunction has been demonstrated to be a key pathogenic step in the initiation and progression of neurological deficits [46, 47]. As the core constituent of the BBB, BMEC dysfunction alone is sufficient to promote BBB defects, and evidence for its destruction exists in various neurodegenerative diseases, including AD, Parkinson disease (PD) and amyotrophic lateral sclerosis (ALS) [48–50]. A previous study has reported that CUMS could inhibit the proliferation, migration, and angiogenesis of BMECs [51]. Here, our in vitro results showed that rutin promoted the proliferation, migration and tube formation of BMECs under GC stimulation, implicating the role of rutin in recovering BMEC functionality after exposure to chronic stress. Notably, the optimal maintenance of the BBB necessitates coordinated crosstalk between BMECs and other cells in the neurovascular unit (NVU) [52]. Further investigations of the mechanism underlying the effects of rutin should consider cell–to–cell contacts to better understand its neuroprotective potential.

In–depth explorations regarding the molecular mechanisms of rutin in neuroprotection is of great necessity for expanding its clinical applications. Unlike peripheral endothelial cells, BMECs express specialized intercellular TJs to maintain low paracellular permeability [53]. Claudin–5 is the dominant component of TJ proteins and is indispensable for BMEC integrity [54]. Loss of Claudin–5 leads to the breakdown of BBB and disruption of the brain microenvironment [54, 55]. Our recent study complements a series of studies showing that BBB decomposition reflected by Claudin–5 decline is sufficient to elicit neurobehavioral alterations under chronic stress [29, 37, 56, 57]. Moreover, the epigenetic patterns of Claudin–5 have been shown to be correlated with the pathogenesis of cognitive decline [37, 38, 58], highlighting the importance of Claudin–5 expression in maintaining the normal function of the CNS. Therefore, the discovery of novel drug targets to restore neurovascular health may reduce the pathologies of CNS diseases. A major impediment to this goal is the lack of therapeutic agents that can enhance Claudin–5 expression to repair BBB damage, as no such compounds exist thus far in clinic. Herein, we demonstrated that rutin inhibited HDAC1–dependent histone deacetylation and thus facilitated the activation of C/EBPα on the *Cldn5* gene transcription. As a result, rutin treatment reversed Claudin–5 loss and endothelium damage, thus alleviating cognitive deficits in CUMS model mice. Importantly, histone acetylation has been proposed as one of the main epigenetic modifications that contribute to the pathologic mechanisms of cognitive decline. Abnormal histone acetylation such as H3K27ac is proved to correlate with Aβ and tau pathology in the prefrontal cortex of AD patients [59]. HDAC inhibitors including vorinostat (SAHA) and valproic acid (VPA) are able to facilitate the transcription of genes involved in synaptic plasticity and reverse long–term memory impairments [60, 61], bringing promising results for the therapeutics of cognitive decline. A handful of studies have indicated the participation of rutin and its derivatives in the regulation of histone acetylation [45, 62–64]. Using drug repurposing strategy, our present study identified that rutin possess HDAC1 inhibition ability to facilitate neurovascular H3K27ac modification. Given the importance of histone acetylation in neurological functions, the interplay of rutin with histone acetylation modifiers in other models of cognitive decline should attract more attention and warrants further research.

Inflammation is both a cause and a result of BBB disruption. Inflammatory responses caused by chronic stress compromise BBB integrity [65], and in turn, the loss of Claudin–5 and leaky BBB result in the infiltration of proinflammatory cytokines into the brain [66]. Previous studies have highlighted the significance of rutin in protecting against neuroinflammation [67, 68]; however, the anti–inflammatory roles of rutin remain not fully understood. Herein, we found that the restoration of rutin on the BBB could hinder the accumulation of circulating proinflammatory cytokines in stress–related regions. Notably, the direct inhibitory effect of rutin on the production and release of proinflammatory factors may also contribute to its influence on BBB function [69–71]. Considering the neuroprotective activity of rutin, a greater understanding of the mechanisms by which rutin repairs neurovascular damage induced by chronic stress can promote the design of more effective strategies for treating cognitive impairments. It is also worthing that the limited solubility and unsatisfactory bioavailability of rutin remain substantial challenges for its clinical use [39]. Effective strategies to improve the oral absorption of rutin, such as converting it to the salt formation or loading into nanoparticles [15, 40], need to be further developed to release its ultimate therapeutic potency.

Conclusions

In summary, we revealed the contribution of rutin to restoring stress–induced BBB damage and cognitive deficits. Rutin leads to the recovery of BMEC function, including proliferation, migration and tube formation, through regulating the expression of genes involved in theses processes. Additionally, rutin activates hippocampal *Cldn5* transcription epigenetically and stabilizes BBB integrity. Our study provides strong evidence of the positive regulatory effect of rutin on BBB function and identifies tantalizing therapies for stress–induced cognitive impairments.

Abbreviations

AD	Alzheimer's disease
ALS	Amyotrophic lateral sclerosis
BBB	Blood–brain barrier
BCA	Bicinchoninic acid
BMECs	Brain microvascular endothelial cells
ChIP	Chromatin immunoprecipitation
CMC	Carboxymethyl cellulose
CNS	Central nervous system
CUMS	Chronic unpredictable mild stress
DEGs	Differentially expressed genes
FBS	Fetal bovine serum
FITC	Fluorescein isothiocyanate
GC	Glucocorticoid
GO	Gene ontology
HDAC1	Histone deacetylase 1
MACS	Magnetic–activated cell sorting
MWM	Morris water maze
NaFI	Sodium fluorescein
NORT	Novel object recognition test
NVU	Neurovascular unit
PBS	Phosphate–buffered saline
PD	Parkinson's disease
PFA	Paraformaldehyde
PVDF	Polyvinylidene difluoride
qRT–PCR	Quantitative real–time PCR
SEM	Standard error of the mean
TEER	Trans-endothelial electrical resistance
TEM	Transmission electron microscopy
TJs	Tight junctions
TNF–α	Tumor necrosis factor–α
TSS	Transcription start site

Supplementary Information

The online version contains supplementary material available at https://doi.org/10.1186/s12987-025-00639-8.

Additional file 1.

Additional file 2.

Additional file 3.

Additional file 4.

Additional file 5.

Acknowledgements

Not applicable.

Author contributions

Z. –W. S., Y. Z., F. X., X. W., H. F., and L. –J. Q. conceived the research and analyzed and interpreted the data. Z. –W. S., Z. –X. S., Y. Z., L. Z., J. –S. L. and M. –Y. Z designed and performed the experiments. Z. –W. S, Z. –X. S., Y. Z., H. F. and L. –J. Q drafted and revised the manuscript. All the authors read and approved the final manuscript.

Funding

This work was supported by the National Natural Science Foundation of China [Grant Number 82201685].

Availability of data and materials

The RNA–seq data generated and analyzed during the current study are available in the GEO repository and the accession number is GSE288810.

Declarations

Ethics approval and consent to participate

All animal experiments and experimental procedures were authorized by the Animal Care and Use Committee at the AMS (IACUC-DWZX-2022–738).

Consent for publication

Not applicable.

Competing interests

The authors declare no competing interests.

Author details

[1]Beijing Institute of Basic Medical Sciences, Beijing 100850, China. [2]Tianjin Key Laboratory of Exercise Physiology and Sports Medicine, Institute of Sport, Exercise & Health, Tianjin University of Sport, Tianjin 301617, China.

Received: 18 December 2024 Accepted: 10 March 2025
Published online: 02 April 2025

References

1. Saeedi M, Rashidy-Pour A. Association between chronic stress and Alzheimer's disease: therapeutic effects of Saffron. Biomed Pharmacother. 2021;133:110995.
2. Lupien SJ, Juster RP, Raymond C, Marin MF. The effects of chronic stress on the human brain: from neurotoxicity, to vulnerability, to opportunity. Front Neuroendocrinol. 2018;49:91–105.
3. Escher CM, Sannemann L, Jessen F. Stress and Alzheimer's disease. J Neural Transm. 2019;126:1155–61.
4. Lyons CE, Bartolomucci A. Stress and Alzheimer's disease: a senescence link? Neurosci Biobehav Rev. 2020;115:285–98.
5. Zhang YL, Wang J, Zhang ZN, Su Q, Guo JH. The relationship between amyloid-beta and brain capillary endothelial cells in Alzheimer's disease. Neural Regen Res. 2022;17:2355–63.
6. Liu Y, Zhang T, Meng D, Sun L, Yang G, He Y, et al. Involvement of CX3CL1/CX3CR1 in depression and cognitive impairment induced by chronic unpredictable stress and relevant underlying mechanism. Behav Brain Res. 2020;381:112371.
7. Knox EG, Aburto MR, Clarke G, Cryan JF, O'Driscoll CM. The blood-brain barrier in aging and neurodegeneration. Mol Psychiatry. 2022;27:2659–73.
8. Hashimoto Y, Greene C, Munnich A, Campbell M. The CLDN5 gene at the blood-brain barrier in health and disease. Fluids Barriers CNS. 2023;20:22.
9. Cortes A, Solas M, Pejenaute A, Abellanas MA, Garcia-Lacarte M, Aymerich MS, et al. Expression of endothelial NOX5 alters the integrity of the blood-brain barrier and causes loss of memory in aging mice. Antioxidants. 2021;10:1311.
10. Puech C, Badran M, Runion AR, Barrow MB, Cataldo K, Gozal D. Cognitive impairments, neuroinflammation and blood-brain barrier permeability in mice exposed to chronic sleep fragmentation during the daylight period. Int J Mol Sci. 2023;24:9880.
11. Parashar A, Mehta V, Udayabanu M. Rutin alleviates chronic unpredictable stress-induced behavioral alterations and hippocampal damage in mice. Neurosci Lett. 2017;656:65–71.
12. Ding MR, Qu YJ, Hu B, An HM. Signal pathways in the treatment of Alzheimer's disease with traditional Chinese medicine. Biomed Pharmacother. 2022;152:113208.

13. Kennedy DO, Bonnländer B, Lang SC, Pischel I, Forster J, Khan J, et al. Acute and chronic effects of green oat (Avena sativa) extract on cognitive function and mood during a laboratory stressor in healthy adults: a randomised, double-blind, placebo-controlled study in healthy humans. Nutrients. 2020;12:1598.
14. Sun XY, Li LJ, Dong QX, Zhu J, Huang YR, Hou SJ, et al. Rutin prevents tau pathology and neuroinflammation in a mouse model of Alzheimer's disease. J Neuroinflammation. 2021;18:131.
15. Pan RY, Ma J, Kong XX, Wang XF, Li SS, Qi XL, et al. Sodium rutin ameliorates Alzheimer's disease-like pathology by enhancing microglial amyloid-β clearance. Sci Adv. 2019;5:eaau6328.
16. Ramalingayya GV, Cheruku SP, Nayak PG, Kishore A, Shenoy R, Rao CM, et al. Rutin protects against neuronal damage in vitro and ameliorates doxorubicin-induced memory deficits in vivo in Wistar rats. Drug Des Devel Ther. 2017;11:1011–26.
17. Hasanein P, Emamjomeh A, Chenarani N, Bohlooli M. Beneficial effects of rutin in diabetes-induced deficits in acquisition learning, retention memory and pain perception in rats. Nutr Neurosci. 2020;23:563–74.
18. Yang Y, Bai L, Li X, Xiong J, Xu P, Guo C, et al. Transport of active flavonoids, based on cytotoxicity and lipophilicity: an evaluation using the blood-brain barrier cell and Caco-2 cell models. Toxicol In Vitro. 2014;28:388–96.
19. Wang X, Zhao X, Feng T, Jin G, Li Z. Rutin prevents high glucose-induced renal glomerular endothelial hyperpermeability by inhibiting the ROS/Rhoa/ROCK signaling pathway. Planta Med. 2016;82:1252–7.
20. Jang JW, Lee JK, Hur H, Kim TW, Joo SP, Piao MS. Rutin improves functional outcome via reducing the elevated matrix metalloproteinase-9 level in a photothrombotic focal ischemic model of rats. J Neurol Sci. 2014;339:75–80.
21. Rodrigues AM, Marcilio Fdos S, Frazão Muzitano M, Giraldi-Guimarães A. Therapeutic potential of treatment with the flavonoid rutin after cortical focal ischemia in rats. Brain Res. 2013;1503:53–61.
22. Wang SD, Wang X, Zhao Y, Xue BH, Wang XT, Chen YX, et al. Homocysteine-induced disturbances in DNA methylation contribute to development of stress-associated cognitive decline in rats. Neurosci Bull. 2022;38:887–900.
23. Weksler B, Romero IA, Couraud PO. The hCMEC/D3 cell line as a model of the human blood brain barrier. Fluids Barriers CNS. 2013;10:16.
24. Li S, Hu W, Gong S, Zhang P, Cheng J, Wang S, et al. The role of PRRC2B in cerebral vascular remodeling under acute hypoxia in mice. Adv Sci. 2023;10:e2300892.
25. Cui Q, Zhang Y, Tian N, Yang J, Ya D, Xiang W, et al. Leptin promotes angiogenesis via pericyte STAT3 pathway upon intracerebral hemorrhage. Cells. 2022;11:2755.
26. Greene C, Hanley N, Reschke CR, Reddy A, Mae MA, Connolly R, et al. Microvascular stabilization via blood-brain barrier regulation prevents seizure activity. Nat Commun. 2022;13:2003.
27. Pan RY, He L, Zhang J, Liu X, Liao Y, Gao J, et al. Positive feedback regulation of microglial glucose metabolism by histone H4 lysine 12 lactylation in Alzheimer's disease. Cell Metab. 2022;34:634-48.e6.
28. Zhao Z, Yu Z, Hou Y, Zhang L, Fu A. Improvement of cognitive and motor performance with mitotherapy in aged mice. Int J Biol Sci. 2020;16:849–58.
29. Menard C, Pfau ML, Hodes GE, Kana V, Wang VX, Bouchard S, et al. Social stress induces neurovascular pathology promoting depression. Nat Neurosci. 2017;20:1752–60.
30. Cheng Y, Desse S, Martinez A, Worthen RJ, Jope RS, Beurel E. TNFα disrupts blood brain barrier integrity to maintain prolonged depressive-like behavior in mice. Brain Behav Immun. 2018;69:556–67.
31. Zenaro E, Piacentino G, Constantin G. The blood-brain barrier in Alzheimer's disease. Neurobiol Dis. 2017;107:41–56.
32. Rajeev V, Fann DY, Dinh QN, Kim HA, De Silva TM, Lai MKP, et al. Pathophysiology of blood brain barrier dysfunction during chronic cerebral hypoperfusion in vascular cognitive impairment. Theranostics. 2022;12:1639–58.
33. Wang W, Wu QH, Sui Y, Wang Y, Qiu X. Rutin protects endothelial dysfunction by disturbing Nox4 and ROS-sensitive NLRP3 inflammasome. Biomed Pharmacother. 2017;86:32–40.
34. Zhao T, He F, Zhao K, Yuxia L, Li H, Liu X, et al. A triple-targeted rutin-based self-assembled delivery vector for treating ischemic stroke by vascular normalization and anti-inflammation via ACE2/Ang1-7 signaling. ACS Cent Sci. 2023;9:1180–99.
35. Zhang ZQ, Wang X, Xue BH, Zhao Y, Xie F, Wang SD, et al. Chronic stress promotes glioma cell proliferation via the PI3K/Akt signaling pathway. Oncol Rep. 2021. https://doi.org/10.3892/or.2021.8153.
36. ZhiQing Z, XinXing W, Jingbo G, Rui Z, Xiujie G, Yun Z, et al. Effects of HIP in protection of HSP70 for stress-induced cardiomyocytes injury and its glucorticoid receptor pathway. Cell Stress Chaperones. 2014;19:865–75.
37. Sun ZW, Wang X, Zhao Y, Sun ZX, Wu YH, Hu H, et al. Blood-brain barrier dysfunction mediated by the EZH2-Claudin-5 axis drives stress-induced TNF-α infiltration and depression-like behaviors. Brain Behav Immun. 2024;115:143–56.
38. Dudek KA, Dion-Albert L, Lebel M, LeClair K, Labrecque S, Tuck E, et al. Molecular adaptations of the blood-brain barrier promote stress resilience vs. depression. Proc Natl Acad Sci USA. 2020;117:3326–36.
39. Li B, Yu Y, Liu K, Zhang Y, Geng Q, Zhang F, et al. β-Hydroxybutyrate inhibits histone deacetylase 3 to promote claudin-5 generation and attenuate cardiac microvascular hyperpermeability in diabetes. Diabetologia. 2021;64:226–39.
40. Kakogiannos N, Ferrari L, Giampietro C, Scalise AA, Maderna C, Ravà M, et al. JAM-A acts via C/EBP-α to promote claudin-5 expression and enhance endothelial barrier function. Circ Res. 2020;127:1056–73.
41. Zhang L, Wang J. Sinomenine alleviates glomerular endothelial permeability by activating the C/EBP-α/claudin-5 signaling pathway. Hum Cell. 2022;35:1453–63.
42. Man YG, Zhou RG, Zhao B. Efficacy of rutin in inhibiting neuronal apoptosis and cognitive disturbances in sevoflurane or propofol exposed neonatal mice. Int J Clin Exp Med. 2015;8:14397–409.
43. Xu PX, Wang SW, Yu XL, Su YJ, Wang T, Zhou WW, et al. Rutin improves spatial memory in Alzheimer's disease transgenic mice by reducing Aβ oligomer level and attenuating oxidative stress and neuroinflammation. Behav Brain Res. 2014;264:173–80.
44. Emudainohwo JOT, Ben-Azu B, Adebayo OG, Aduema W, Uruaka C, Ajayi AM, et al. Normalization of HPA axis, cholinergic neurotransmission, and inhibiting brain oxidative and inflammatory dynamics are associated with the adaptogenic-like effect of rutin against psychosocial defeat stress. J Mol Neurosci. 2023;73:60–75.
45. Javed H, Khan MM, Ahmad A, Vaibhav K, Ahmad ME, Khan A, et al. Rutin prevents cognitive impairments by ameliorating oxidative stress and neuroinflammation in rat model of sporadic dementia of Alzheimer type. Neuroscience. 2012;210:340–52.
46. Greene C, Connolly R, Brennan D, Laffan A, O'Keeffe E, Zaporojan L, et al. Blood-brain barrier disruption and sustained systemic inflammation in individuals with long COVID-associated cognitive impairment. Nat Neurosci. 2024;27:421–32.
47. Sweeney MD, Zhao Z, Montagne A, Nelson AR, Zlokovic BV. Blood-brain barrier: from physiology to disease and back. Physiol Rev. 2019;99:21–78.
48. Jia G, Aroor AR, Jia C, Sowers JR. Endothelial cell senescence in aging-related vascular dysfunction. Biochim Biophys Acta Mol Basis Dis. 2019;1865:1802–9.
49. Graves SI, Baker DJ. Implicating endothelial cell senescence to dysfunction in the ageing and diseased brain. Basic Clin Pharmacol Toxicol. 2020;127:102–10.
50. Peeyush Kumar T, McBride DW, Dash PK, Matsumura K, Rubi A, Blackburn SL. Endothelial cell dysfunction and injury in subarachnoid hemorrhage. Mol Neurobiol. 2019;56:1992–2006.
51. Zhang S, Lu Y, Shi W, Ren Y, Xiao K, Chen W, et al. SIRT1/FOXO1 axis-mediated hippocampal angiogenesis is involved in the antidepressant effect of Chaihu Shugan San. Drug Des Devel Ther. 2022;16:2783–801.
52. Kaplan L, Chow BW, Gu C. Neuronal regulation of the blood-brain barrier and neurovascular coupling. Nat Rev Neurosci. 2020;21:416–32.
53. Boyé K, Geraldo LH, Furtado J, Pibouin-Fragner L, Poulet M, Kim D, et al. Endothelial Unc5B controls blood-brain barrier integrity. Nat Commun. 2022;13:1169.
54. Ma SC, Li Q, Peng JY, Zhouwen JL, Diao JF, Niu JX, et al. Claudin-5 regulates blood-brain barrier permeability by modifying brain microvascular endothelial cell proliferation, migration, and adhesion to prevent lung cancer metastasis. CNS Neurosci Ther. 2017;23:947–60.
55. Chiba H, Ichikawa-Tomikawa N, Imura T, Sugimoto K. The region-selective regulation of endothelial claudin-5 expression and signaling in brain health and disorders. J Cell Physiol. 2021;236:7134–43.

56. Wang Q, Huang X, Su Y, Yin G, Wang S, Yu B, et al. Activation of Wnt/β-catenin pathway mitigates blood-brain barrier dysfunction in Alzheimer's disease. Brain. 2022;145:4474–88.
57. Zhu N, Wei M, Yuan L, He X, Chen C, Ji A, et al. Claudin-5 relieves cognitive decline in Alzheimer's disease mice through suppression of inhibitory GABAergic neurotransmission. Aging. 2022;14:3554–68.
58. Hüls A, Robins C, Conneely KN, Edgar R, De Jager PL, Bennett DA, et al. Brain DNA methylation patterns in CLDN5 associated with cognitive decline. Biol Psychiatry. 2022;91:389–98.
59. Santana DA, Smith MAC, Chen ES. Histone modifications in Alzheimer's disease. Genes. 2023;14:347.
60. Sgobio C, Ghiglieri V, Costa C, Bagetta V, Siliquini S, Barone I, et al. Hippocampal synaptic plasticity, memory, and epilepsy: effects of long-term valproic acid treatment. Biol Psychiatry. 2010;67:567–74.
61. Wong LW, Chong YS, Wong WLE, Sajikumar S. Inhibition of histone deacetylase reinstates hippocampus-dependent long-term synaptic plasticity and associative memory in sleep-deprived mice. Cereb Cortex. 2020;30:4169–82.
62. Zhang ZF, Zhang YQ, Fan SH, Zhuang J, Zheng YL, Lu J, et al. Troxerutin protects against 2,2′,4,4′-tetrabromodiphenyl ether (BDE-47)-induced liver inflammation by attenuating oxidative stress-mediated NAD^+-depletion. J Hazard Mater. 2015;283:98–109.
63. Çetin Ö, Sari S, Erdem-Yurter H, Bora G. Rutin increases alpha-tubulin acetylation via histone deacetylase 6 inhibition. Drug Dev Res. 2022;83:993–1002.
64. Dong R, Zhang X, Liu Y, Zhao T, Sun Z, Liu P, et al. Rutin alleviates EndMT by restoring autophagy through inhibiting HDAC1 via PI3K/AKT/mTOR pathway in diabetic kidney disease. Phytomedicine. 2023;112:154700.
65. Huang X, Hussain B, Chang J. Peripheral inflammation and blood-brain barrier disruption: effects and mechanisms. CNS Neurosci Ther. 2021;27:36–47.
66. Greene C, Hanley N, Reschke CR, Reddy A, Mäe MA, Connolly R, et al. Microvascular stabilization via blood-brain barrier regulation prevents seizure activity. Nat Commun. 2022;13:2003.
67. Muvhulawa N, Dludla PV, Ziqubu K, Mthembu SXH, Mthiyane F, Nkambule BB, et al. Rutin ameliorates inflammation and improves metabolic function: a comprehensive analysis of scientific literature. Pharmacol Res. 2022;178:106163.
68. Wang J, Yu Z, Peng Y, Xu B. Insights into prevention mechanisms of bioactive components from healthy diets against Alzheimer's disease. J Nutr Biochem. 2023;119:109397.
69. Lu W, Chen Z, Wen J. Flavonoids and ischemic stroke-induced neuroinflammation: focus on the glial cells. Biomed Pharmacother. 2024;170:115847.
70. Wang M, Ma X, Gao C, Luo Y, Fei X, Zheng Q, et al. Rutin attenuates inflammation by downregulating AGE-RAGE signaling pathway in psoriasis: network pharmacology analysis and experimental evidence. Int Immunopharmacol. 2023;125:111033.
71. Oluranti OI, Alabi BA, Michael OS, Ojo AO, Fatokun BP. Rutin prevents cardiac oxidative stress and inflammation induced by bisphenol A and dibutyl phthalate exposure via NRF-2/NF-κB pathway. Life Sci. 2021;284:119878.

Publisher's Note